Shi, Y. et al. (2014) *High channel count and high precision channel spacing multi-wavelength laser array for future PICs.* Scientific Reports, 4 . p. 7377. ISSN 2045-2322

http://eprints.gla.ac.uk/99573/

Deposited on: 19 December 2014

OPEN

High channel count and high precision channel spacing multi-wavelength laser array for future PICs

Yuechun Shi[1], Simin Li[1,2], Xiangfei Chen[1], Lianyan Li[1,3], Jingsi Li[4], Tingting Zhang[1], Jilin Zheng[1], Yunshan Zhang[1], Song Tang[1], Lianping Hou[2], John H. Marsh[2] & Bocang Qiu[5]

[1]National Laboratory of Solid State Microstructures, College of Engineering and Applied Sciences, Microwave-Photonics Technology Laboratory, Nanjing University, Nanjing, 210093, China, [2]School of Engineering, University of Glasgow, Glasgow G12 8QQ, U.K, [3]Photonics Research Group, Department of Information Technology (INTEC), Ghent University, Sint-Pietersnieuwstraat 41, 9000 Ghent, Belgium, [4]Microelectronic Research Center, Department of Electrical Engineering, The University of Texas at Austin, Austin, Texas 78758, USA, [5]Suzhou Institute of Nano-Tech and Nano-Bionics, Chinese Academy of Sciences, Suzhou 215123, China.

Multi-wavelength semiconductor laser arrays (MLAs) have wide applications in wavelength multiplexing division (WDM) networks. In spite of their tremendous potential, adoption of the MLA has been hampered by a number of issues, particularly wavelength precision and fabrication cost. In this paper, we report high channel count MLAs in which the wavelengths of each channel can be determined precisely through low-cost standard μm-level photolithography/holographic lithography and the reconstruction-equivalent-chirp (REC) technique. 60-wavelength MLAs with good wavelength spacing uniformity have been demonstrated experimentally, in which nearly 83% lasers are within a wavelength deviation of ±0.20 nm, corresponding to a tolerance of ±0.032 nm in the period pitch. As a result of employing the equivalent phase shift technique, the single longitudinal mode (SLM) yield is nearly 100%, while the theoretical yield of standard DFB lasers is only around 33.3%.

Since the proposal of the concept of photonic integrated circuits (PICs), tremendous progress has been made. In 2005, Infinera Corp. rolled out the first commercial PICs, in which hundreds of optical functions were integrated onto a small form factor chip for wavelength multiplexing division (WDM) systems[1], and a monolithically integrated 5×100 Gb/s WDM chip has now been demonstrated. Despite the advances made in recent years, there are still some general challenges associated with PICs, such as materials[2,3], integration of the isolators[4], and ultra-low-cost fabrication[5]. Of the issues indicated above, the critical issue to be addressed is how to increase the integration density at a very low cost. Multi-wavelength laser arrays (MLAs) with a high channel count are considered to be an engine of PICs, but high-volume production of MLAs with accurate wavelength control and low manufacturing cost remains a huge challenge. Currently, the distributed feedback (DFB) lasers used in MLAs are fabricated using electron beam lithography (EBL), which offers high resolution fabrication but low throughput because of the long writing time[6]. It is also well-known that EBL suffers from drawbacks such as blanking or deflection errors and shaping errors. Very few references have discussed the non-uniformity of the wavelength spacing of the devices fabricated using EBL. In Ref. 6, it is shown that using EBL, only 35% lasers have a wavelength variation of less than ±0.2 nm. To the best of our knowledge, this is the most recent paper reporting a statistically significant data set concerning wavelength accuracy. Ref. 7 shows that the error associated with the EBL process may be as large as 3 nm. No further reports with detailed information are available. Such issues greatly decrease the yield of monolithically integrated WDM PICs and significantly increase their manufacturing cost.

The yield and cost of DFB laser arrays are considerably different from those of individual lasers. At present, the manufacturing cost of an individual laser is very low. However, when the yield is 80% for an individual component, the yield of a 60-laser array is only around 0.0015%, and the cost will be several tens of thousand times more than that of the individual lasers, which makes it impossible to manufacture high-channel-count, monolithically integrated WDM chips. Furthermore the fine wavelength tuning required for each channel can only be accomplished using a sophisticated chip structure and complex auxiliary systems, leading to extra power consumption and degraded laser performances[8].

The yield issue is one of the major obstacles in manufacturing ultra-large scale PICs. In this paper, 60-channel WDM laser arrays based on the reconstruction-equivalent-chirp (REC) technique are reported, in which nearly 83% of the lasers are within a wavelength deviation of ±0.20 nm. Furthermore, the lasers are fabricated using only standard commercial semiconductor processes and μm-level photolithography. The good experimental results imply that the two great obstacles to manufacture MLAs for very-large-scale PICs, namely poor wavelength accuracy and the low yield, which have impeded progress for nearly three decades, have been essentially overcome.

Results

Principle of the REC technique. Although the basic principle of REC has been well illustrated[9,10], here the REC technique is further explained by a new view of the well-known wave-vector conservation principle. The grating-vector conversion relation in a sampled grating with a uniform seed (basic) grating and arbitrary sampling pattern can be expressed as,

$$K_g(z) = K_0 + K_s(z) \text{ or } \frac{1}{\Lambda_m(z)} = \frac{1}{\Lambda_0(z)} + \frac{mf'(z)}{P} \quad (1)$$

Here K_g is the wave-vector of the mth order sub-grating of the sampled grating, K_s is the wave-vector of the mth order Fourier component of the sampling pattern, and K_0 is the wave-vector of the seed grating. $f(z)$ describes the arbitrary profile of the sampling pattern. P is the reference sampling period, which is of μm scale. From equation (1), it can be seen that an additional component $\frac{mf'(z)}{P}$ with large scale of P is introduced to manipulate the grating structure.

As illustrated in Fig. 1, an additional wave-vector $K_s(z)$, resulting from the large scale sampling pattern, is introduced artificially. Hence, the wave-vector of the sampled grating $K_g(z)$ can be manipulated by altering the value of $K_s(z)$. If the phase match condition between the light and $K_g(z)$ is satisfied, the interaction takes place. As a consequence, the optical properties of the grating can be equivalently realized by designing a μm-scale sampling pattern, and the wavelength precision can be improved by a factor of $mf'(z)/(P/\Lambda_0 + mf'(z))^2$ [11,12]. Therefore, the fabrication tolerance can be relaxed and the fabrication cost can be dramatically reduced. This principle is very similar to quasi-phase matching (QPM) in nonlinear materials for high efficiency light wavelength conversion[13,14], where an artificial periodic structure with larger period is introduced to produce a desired phase matching condition. So the basic principle of the REC technique can be regarded as microstructure based QPM.

DFB laser array based on REC technique. 60-wavelength DFB laser arrays with a π-equivalent phase shift (π-EPS) were designed and fabricated. The Bragg wavelength of the 0th order sub-grating is about 1640 nm (seed grating period is about 258.7 nm), a wavelength where the gain is small enough to avoid unwanted lasing. The designed wavelength spacing of the arrays is 0.2 nm, 0.4 nm and 0.8 nm, respectively. The sampling periods for 0.8 nm wavelength spacing are from about 2.82 μm to 4.58 μm. The cavity length is

600 μm and the lateral pitch of lasers is 125 μm. A 2 μm ridge waveguide is used to guide light and <1.0% Anti-reflection facet coatings (AR/AR) are applied to avoid the influence of random phase reflections from the facets. The normalized coupling coefficient of the ±1ˢᵗ sub-grating is around 2.5. Fig. 2 shows a schematic illustration of the DFB laser array with π-EPS.

Wavelength accuracy performances of the arrays. DFB MLAs were fabricated on two wafers with different seed grating periods. Seven 60-wavelength MLAs from one wafer were randomly selected for a detailed analysis of the lasing wavelength precision. All the lasers were measured at the same bias current of 80 mA and at an ambient temperature of 23°C. The second wafer, with a different seed grating period, was used to verify the effectiveness of the REC technique.

The relative wavelength accuracy was determined as follows. The measured wavelengths of the lasers in arrays were measured and linearly fitted. The wavelength residual, which indicates wavelength deviations (δ) from the fitted line, could then be obtained. The slope of the fitted line denotes the wavelength spacing of the fabricated MLA. The detailed wavelength residual frequency counts of the seven measured arrays are shown in Fig. 3. For all the laser arrays, the mean lasing wavelength residuals of 83.3% of the lasers are within ±0.20 nm, and 93.5% are within ±0.30 nm. Lasers with a wavelength deviation of >0.50 nm are less than 1.0% of the total laser count. The single-longitudinal-mode (SLM) yield of lasers from the seven arrays are 98.3%, 100%, 100%, 100%, 98.3%, 93.3% and 100% respectively, with the average SLM yield being 98.6%.

During cleaving and measurement, some laser bars were damaged, especially for the MLAs with a large channel number. In order to further investigate the lasing wavelength precision, we analyzed the statistics from 871 randomly selected lasers with the seed grating Bragg wavelength of 1,640 nm, among which some of the laser bars were broken but residual lasers within the arrays could be operated. A further 781 lasers from the second wafer with a seed grating Bragg wavelength of 1,660 nm were also randomly selected for comparison. A Gaussian distribution was fitted to the frequency count of the residual wavelengths.

As shown in Fig. 4, the standard deviations are 0.159 nm and 0.147 nm for the two different seed grating periods, which means 68.26% of the laser wavelengths are lied within ±0.159 nm and ±0.147 nm, respectively. The close values of the standard deviations (~0.01 nm difference) shows that the REC method is effective for different seed grating periods, and confirms the flexibility of the fabrication technique.

Absolute wavelength accuracy is another key parameter that must be evaluated. We randomly selected 6 laser array bars with 15 wavelengths, for which the same wavelength spacing of 0.8 nm was obtained, as shown in Fig. 5(a). Fig. 5(b) illustrates the maximum wavelength differences in each channel for the 6 laser arrays, which vary from 0.36 nm to 1.17 nm with a mean value of 0.788 nm (±0.394 nm) and standard deviation of 0.222 nm. It should be noted that the wafer with epitaxy (epi-wafer) is a commercially available product and is briefly described in following part of Methods and the relative distance between two measured arrays may be very large, which would magnify the effects of non-uniformity of the wafer,
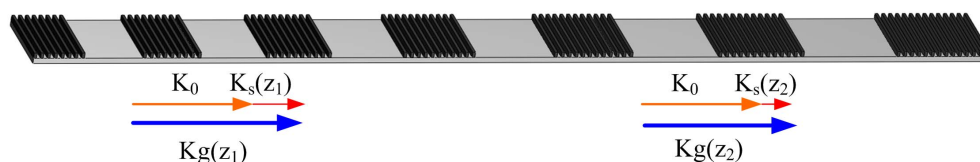
Figure 1 | Schematic illustration of the wave-vector conversion of REC technique. The sampling pattern provides an additional wave-vector $K_s(z)$ to form a new wave-vector of $K_g(z)$ to manipulate the light behavior in a waveguide with uniform seed (basic) grating wave-vector of K_0. Through this vector conversion, complex nanometer grating structures can be equivalently realized by μm-level structures.
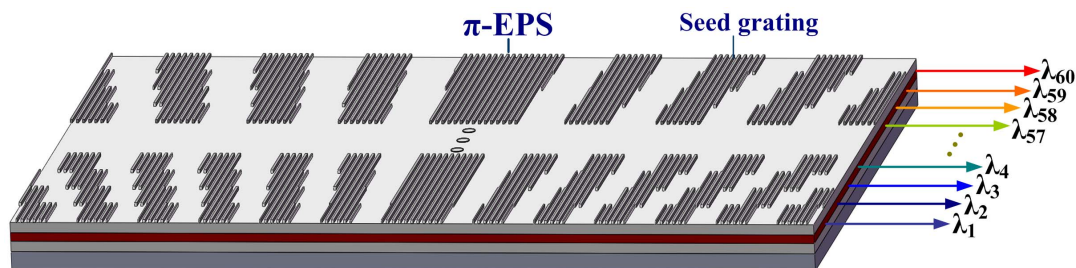
Figure 2 | Schematic of the DFB laser array with π-EPS. The seed grating is uniform with pre-designed sampling pattern with μm-scale for equivalently realizing the nano-fine grating structures. The wavelength can be tailored by sampling period and the single-longitudinal-mode can be guaranteed by π-EPS.

non-uniformity in the holographic lithography and imperfection in fabrication. As a result, the absolute accuracy is worse than the relative wavelength accuracy. However, the deviation of 0.394 nm in the mean absolute wavelength is sufficiently small that it can be easily compensated by adjusting the operating temperature of the chip, as the thermally induced wavelength shift is about 0.09 nm/°C.

An example of 60-wavelength DFB laser array. The detailed lasing spectrum of one array (Array No.5 in Fig. 3) was randomly selected. Its wavelength spacing is 0.8 nm, as shown in Fig. 6(a). One laser out of the 60 elements shows dual mode, so the SLM ratio of the array is as high as 98.3%. Fig. 6(b) shows the lasing wavelengths as well as the linear fitting curve. In order to further analyze the deviation of the measured data from the fitted curve, the wavelength residual values

of 59 lasers (the laser with dual mode was ignored) after fitting is given in Fig. 6(c), which shows that 88% of the laser wavelengths lie within a deviation of ±0.20 nm [Fig. 3 Array No.5 shows detailed information]. The threshold currents are between 25 mA and 35 mA. The high threshold mainly results from the long cavity length (600 μm), and could be reduced by optimizing parameters such as the cavity length, coupling coefficient of the grating, by using a buried-heterostructure waveguide[15].

Discussion

Other than the grating error, some other factors may also influence the wavelength accuracy. These include non-uniformity of the epi-wafer, waveguide inhomogeneity (e.g. width variations) and imperfect facet coatings. The epi-wafer may have spatial variations arising
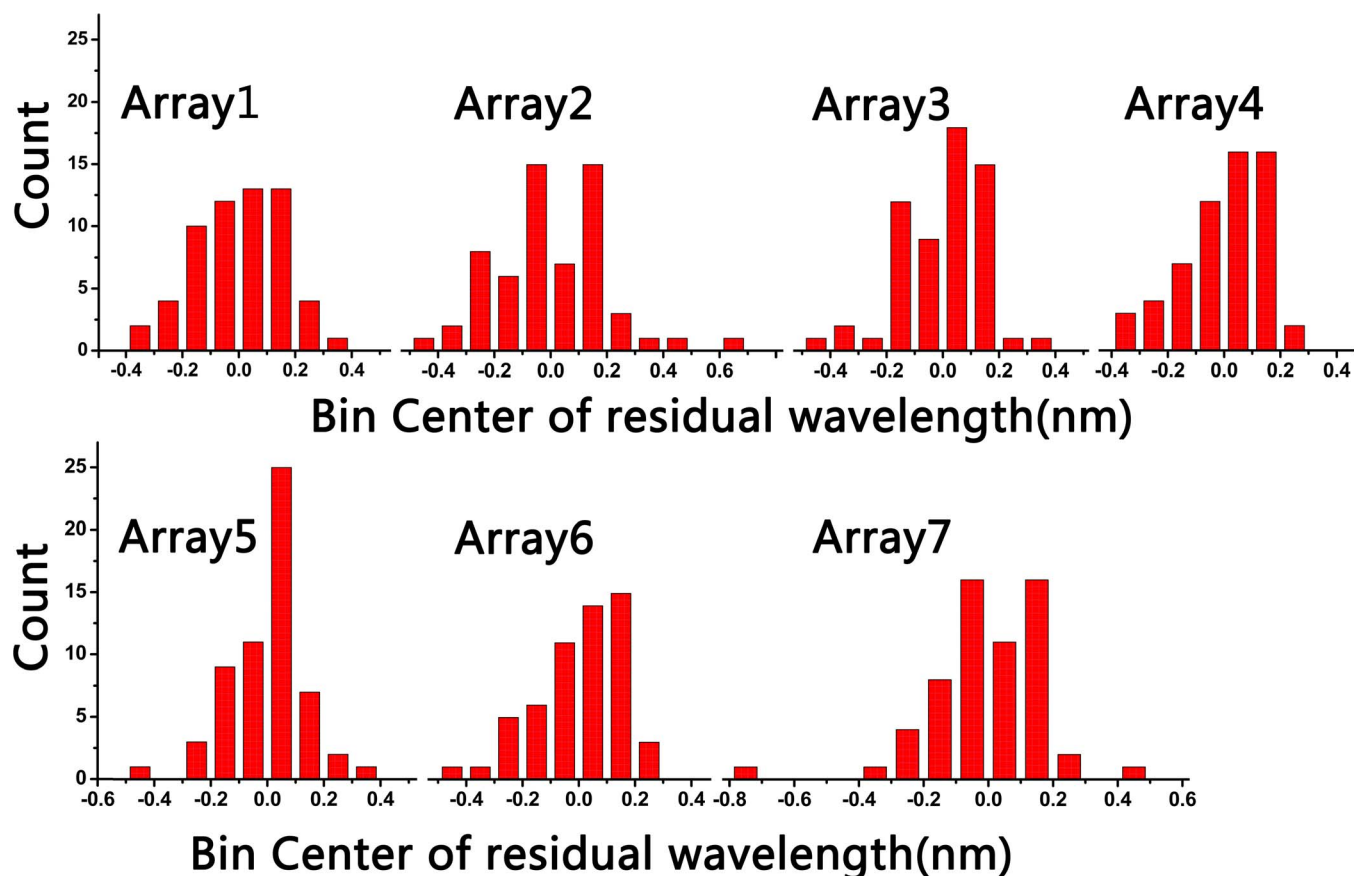
Figure 3 | The statistical characteristics of the measured 7 arrays. The ratios of the wavelength residuals within ±0.20 nm are 81.4%, 71.7%, 90.0%, 85.0% 88.1% 82.1% and 85.0% respectively and the mean value is 83.3%. The single-longitudinal-mode yield of the arrays are 98.3%, 100%, 100%, 100%, 98.3%, 93.3% and 100% respectively.
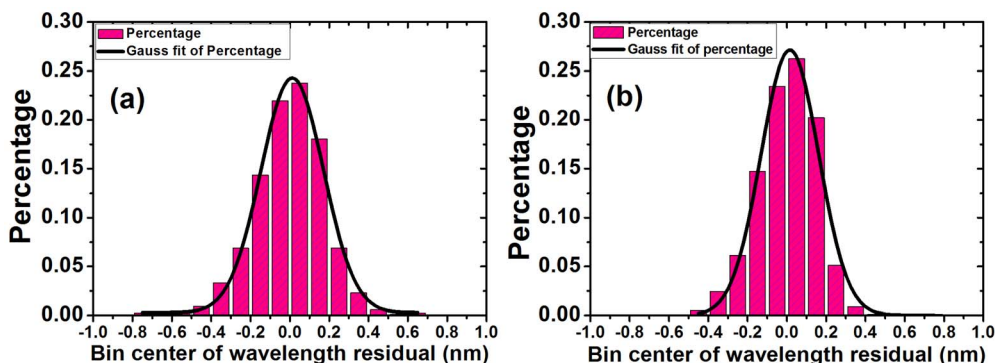
Figure 4 | The frequency count of wavelength residual of (a) 871 lasers with seed grating Bragg wavelength of 1,640 nm and (b) 781 lasers with seed grating Bragg wavelength of 1,660 nm. The standard deviations of the two groups of lasers are 0.159 nm and 0.147 nm respectively.

during material growth. Imperfect fabrication of the waveguide can lead to index variations along its length. In both cases, the lasing wavelength may be slightly shifted. In addition, imperfect facet coatings can lead to residual facet reflections with random phase which can also shift the wavelength. Therefore, in order to further improve the wavelength accuracy, the other processes including material growth, fabrication and post-processing should be improved in the future.

To eliminate the remaining wavelength errors, the absolute wavelength can be readily compensated by changing the temperature of the entire chip by only a few degrees, as already analyzed above. The residual errors in the wavelength spacing can be reduced by improving the fabrication processes or can be compensated directly by fine tuning the injection currents, with a measured current-wavelength slope of about 0.012 nm/mA, to exactly meet the DWDM standard.

DFB laser arrays with grating structures with special properties can also be fabricated using this approach, for example the equivalent of a DFB laser array with 3 phase shifts, which is usually designed for long-cavity narrow-linewidth lasing[12]. It is possible for all the lasers to share the same seed grating, and then various lasers or arrays can be realized simultaneously when defining the sampling patterns. In addition to active components, the REC technique can also be applied to passive filters no matter what material is used[16], where, similarly to the laser array, the Bragg waveguide can also be well controlled[17]. Therefore, both active and passive photonic components can be integrated on the same chip using the REC technique, and the wavelength precision of the active and passive components can be strictly guaranteed simultaneously.

In conclusion, the statistical properties of high channel count DFB laser arrays fabricated using the REC technique have been experimentally studied. Excellent lasing wavelength precision has been achieved. An example of a 60-wavelength DFB laser array has also been demonstrated. All the lasers were fabricated using conventional holographic lithography and photolithography processes; as a result of using the REC technique, high reproducibility is obtained at a remarkably low fabrication cost. Moreover, this technique can also be applied to realize other passive photonic devices based on Bragg grating structures. This report shows that low-cost fabrication of MLAs with high-precision wavelength spacing has been solved. We believe this will provide a platform for volume manufacture of large-scale PICs using a low cost fabrication process based on defining μm-scale features.

Methods

Device fabrication. The laser epi-wafer is fabricated by conventional two-stage low-pressure metal-organic vapor phase epitaxy (MOVPE) with a multiple-quantum-well (MQW) structure as the active region. On an S-doped n-type (100)-oriented InP substrate, an InP buffer layer, a lower AlGaInAs separate-confinement-heterostructure (SCH) layer, a multiple-quantum-well (MQW) structure, an upper AlGaInAs SCH layer, an InP etch stop layer and a 1.25Q InGaAsP grating layer are successively grown. The MQW structure contains five undoped 6nm-thick AlGaInAs quantum well layers with +1.2% compressive strain and six 9nm-thick AlGaInAs barrier layers with -0.45% tensile strain. The photoluminescence (PL) peak of the MQW is around 1540 nm at room temperature. The two SCH layers are asymmetric structure with gradual variations. Then the sampled grating is defined by conventional holographic lithography combined with photolithography. A p-type InP cladding layer and a p-InGaAs contact layer are re-grown. After regrowth, a 2 μm
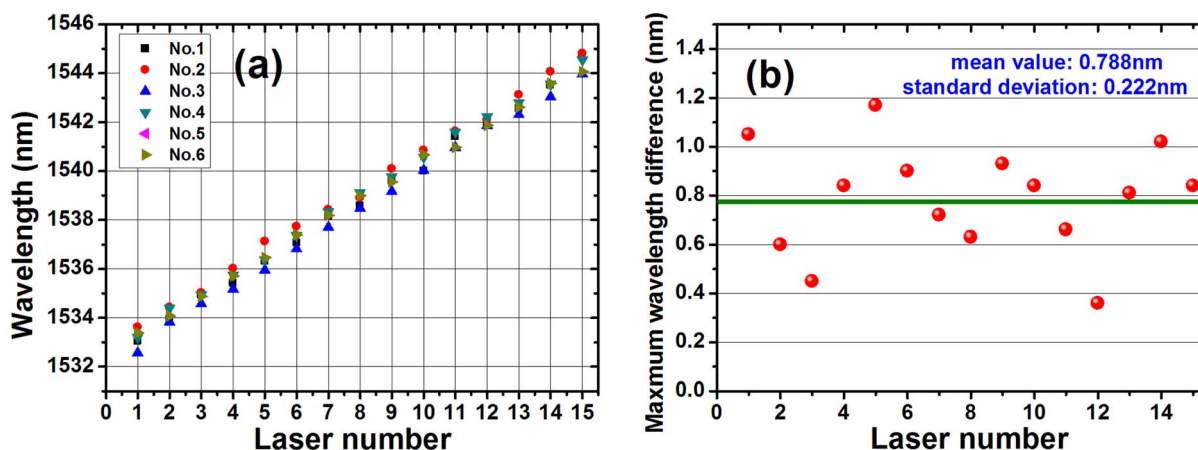
Figure 5 | (a) The lasing wavelengths of 6 laser arrays with wavelength spacing of 0.8 nm. (b) The maximum wavelength differences for the 15 channels of the 6 randomly selected laser arrays. The mean value is 0.788 nm (±0.394 nm) and standard deviation is 0.222 nm.
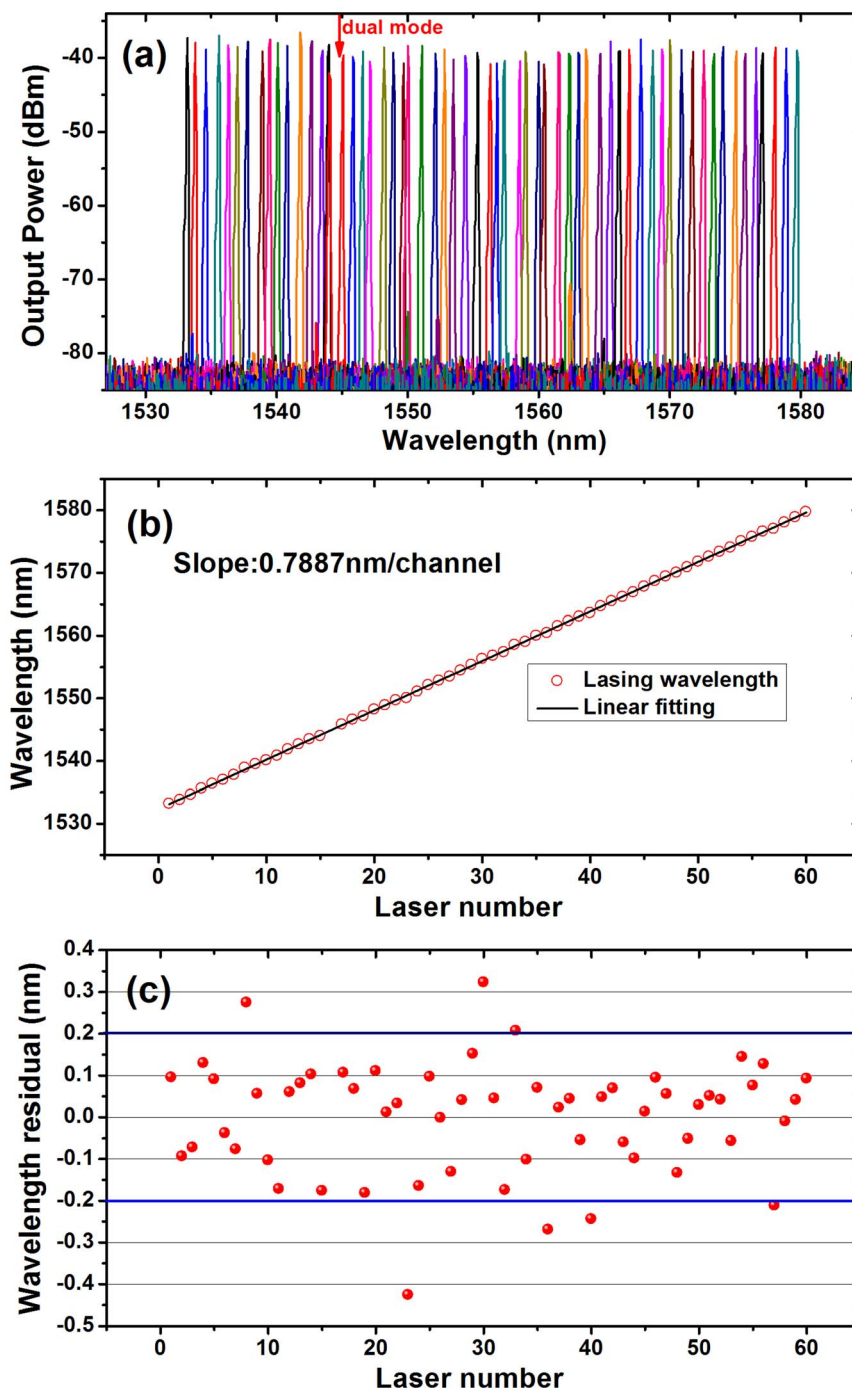
Figure 6 | (a) The measured lasing spectra of one 60-wavelength array which is corresponding to Array No.5 in Fig. 3. One laser is dual mode. (b) The lasing wavelengths and the linear fitting curve with the slope of 0.7887 nm/channel (the deigned value is 0.80 nm/channel). (c) The wavelength residuals after linear fitting which is also plotted in Fig. 3 Array No.5 for detailed statistical data.

ridge waveguide is formed by wet etching. Anti-reflection coatings are deposited on both facets with a reflectivity <1.0%.

1. Nagarajan, R. *et al.* Large-scale photonic integrated circuits. *IEEE J. Sel. Top. Quan. Electron.* **11**, 50–65 (2005).
2. Polman, A. Photonic materials: Teaching silicon new tricks. *Nat. Mater.* **1**, 10–12 (2002).
3. Welch, D. F. *et al.* The realization of large-scale photonic integrated circuits and the associated impact on fiber-optic communication systems. *J. Lightwave Technol.* **24**, 4674–4683 (2006).
4. Oliver, G. Silicon photonics: Integrated isolators. *Nat. Photonics.* **5**, 571–571 (2011).
5. Koch, T. L. & Koren, U. Semiconductor photonic integrated circuits. *IEEE J. Quantum Electron.* **27**, 641–653 (1991).
6. Lee, T.-P. *et al.* Multiwavelength DFB laser array transmitters for ONTC reconfigurable optical network testbed. *J. Lightwave Technol.* **14**, 967–976 (1996).
7. Zanola, M., Strain, M. J., Giuliani, G. & Sorel, M. Post-growth fabrication of multiple wavelength DFB laser arrays with precise wavelengthspacing. *IEEE Photon. Technol. Lett.* **24**, 1063–1065 (2012).
8. Felipe, D. *et al.* Hybrid InP/Polymer optical line terminals for 40-Channel 100-GHz spectrum-sliced WDM-PON. *39th European Conference and Exhibition on Optical Communication (ECOC 2013)*, 237–239; DOI: 10.1049/cp.2013.1352 (2013).
9. Dai, Y. & Chen, X. DFB semiconductor lasers based on reconstruction-equivalent-chirp technology. *Opt. Expr.* **15**, 2348–2353 (2007).
10. Li, J. *et al.* Experimental demonstration of distributed feedback semiconductor lasers based on reconstruction-equivalent-chirp technology. *Opt. Expr.* **17**, 5240–5245 (2009).

11. Shi, Y. *et al.* Experimental demonstration of eight-wavelength distributed feedback semiconductor laser array using equivalent phase shift. *Opt. Lett.* **37**, 3315–3317 (2012).

12. Shi, Y. *et al.* Study of the multiwavelength DFB semiconductor laser array based on the reconstruction-equivalent-chirp technique. *J. Lightwave Technol.* **31**, 3243–3250 (2013).

13. Armstrong, J. A., Bloembergen, N., Ducuing, J. & Pershan, P. S. Interaction between light waves in a nonlinear dielectric. *Phys. Rev.* **127**, 1918–1939 (1962).

14. Zhu, S., Zhu, Y. & Ming, N. Quasi-phase-matched third-harmonic generation in a quasi-periodic optical superlattice. *Science* **278**, 843–846 (1997).

15. Utaka, K., Akiba, S., Sakai, K. & Matsushima, Y. Room-temperature CW operation of distributed-feedback buried-eterostructure InGaAsP/InP lasers emitting at 1.57 μm. *Electron. Lett.* **17**, 961–963 (1981).

16. Sun, J., Holzwarth, C. W. & Smith, H. I. Phase-shift bragg grating in silicon using equivalent phase-shift method. *IEEE Photon. Technol. Lett.* **24**, 25–27 (2012).

17. Sun, J. *et al.* Uniformly spaced λ/4-shifted Bragg grating array with wafer-scale CMOS-compatible process. *Opt. Lett.* **38**, 4002–4004 (2013).

Acknowledgments

Author contributions

Y.S. and X.C. conceived the idea, conducted theoretical analysis. Y.S., X.C. S.L., L.Li, J.L., J.Z. and Y.Z. performed the experiments and analyzed the data. T.Z. and S.T. carried out the measurements. L.H., J.M., B.Q. discussed the experiment results and revised the manuscript. All authors contributed to writing the paper.

Additional information

Competing financial interests: The authors declare no competing financial interests.

How to cite this article: Shi, Y. *et al.* High channel count and high precision channel spacing multi-wavelength laser array for future PICs. *Sci. Rep.* **4**, 7377; DOI:10.1038/srep07377 (2014).